

Determination of Carrier Mobility for Thin-Film Organic and Hybrid Solar Cells through
Transient Photoconductivity

A Thesis

Presented to
the faculty of the School of Engineering and Applied Science
University of Virginia

in partial fulfillment
of the requirements for the degree

Master of Science

by

Angad Singh Sachdeva

August

2014

APPROVAL SHEET

The thesis
is submitted in partial fulfillment of the requirements
for the degree of
Master of Science

Angad Sachdeva 
AUTHOR

The thesis has been read and approved by the examining committee:

Joe C. Campbell

Advisor

Lloyd R. Harriott

Andreas Beling

Accepted for the School of Engineering and Applied Science:



Dean, School of Engineering and Applied Science

August
2014

Abstract

Transient photoconductivity is widely used to study decay characteristics of organic solar cells. For thick devices ($> 1\mu\text{m}$), the Time of Flight (TOF) technique is one such transient technique that is used to extract carrier mobility. TOF determines the amount of time it takes for photon-generated charge carriers to travel from one electrode to another in order to calculate mobility. However, in thin film organic semiconductors, TOF has shown to be difficult to implement due to RC time constant limitations and generation of charge throughout the device.

Recently, transient photoconductivity has been used to measure carrier mobilities in organic thin-film solar cells that reproduced numbers found in literature. To confirm the validity of transient photoconductivity as a means to find mobility, experiments were performed on poly (3-hexylthiophene) (P3HT) and [6,6]-phenyl C61-butyric acid methylester (PCBM) solar cells. The results were compared with Space Charge Limited Current mobility numbers for the same device. Transient photoconductivity was found to be a sound technique under certain conditions. The transient photoconductivity technique was further used to calculate carrier mobility for P3HT:Cadmium Selenide (CdSe) hybrid solar cells, with results agreeing with those found in literature.

Acknowledgment

This thesis is the culmination of two years of research, thought, experiments, successes, failures, hard-work, and reflection. However, I received tremendous guidance, support and help along the way and I would like to acknowledge them in my work.

First, I would like to thank my advisor, Dr. Joe C. Campbell for guiding me at every step. He taught me to think scientifically, encouraged me to work harder, and provided valuable insight on the big questions as well as the small doubts. Dr. Campbell allowed me to come up with my own project and experiment ideas making this endeavor enjoyable and fruitful.

Next, I want to thank my lab colleagues and coworkers for being good friends, keeping the work atmosphere fun amidst all the hours of serious research, and being there to help when I needed them. In particular, I want to thank Kejia Li, Lijun Li, and Yang Shen who have not only been friends but great mentors. They have taught me concepts as well as helped me with my experiments. I would also convey my thanks and sincerest gratitude to Brenda Crider, who was our group secretary for most of my time at the University of Virginia. Brenda's administrative know-how and amicability made sure I never had any problems with paperwork, ordering supplies, or other work-related logistics.

I want to thank Matt Greaney from the University of Southern California for being a great collaborator. Through his busy schedule, Matt found time to fabricate devices and send them over to me each time I requested them. Matt's pace and skill in fabricating solar cells gave me access to a lot of new devices to characterize and study.

I want to say a big thanks to my family and friends who have been great company and the best support system one could ask for. I have had the privilege of being friends with a nice mix of fun, caring, and intellectually stimulating people. To my friends in Charlottesville, Northern Virginia and elsewhere: thank you.

I look up to my parents for their work ethic and positive attitude. They have been an inspiration for me to keep raising the bar professionally and morally. My brother, Surpreet, is the smartest person in our family and I want to thank him for continuously challenging me to think and work smarter. I also owe it to Surpreet for proofreading the two most important documents of my graduate school: my admission essay and my thesis.

Finally, I want to thank my wife, Vidhya, for her unconditional love, support, and guidance. She is my best friend, my most honest critic, and my fiercest competitor. Vidhya has kept my mood bright and my mind focused in the past two years, through the good and the hard times.

Table of Contents

Abstract.....	i
Acknowledgment.....	ii
List of Figures and Tables.....	iv
List of Symbols and Acronyms.....	vi
1. Introduction and Motivation.....	1
2. Device Physics of Organic Solar Cells	3
2.1 Inorganic PN Junction	3
2.2 Organic Solar Cells.....	3
2.2.1 Bilayer vs Bulk Heterojunction	4
3. Carrier Mobility.....	6
3.1 Mobility Measurements in OPVs.....	7
3.1.1 Space Charge Limited Current (SCLC):	7
3.1.2 Charge Extraction by Linearly Increasing Voltage (CELIV)	8
3.1.3 Impedance Spectroscopy.....	9
3.1.4 Transient Photoconductivity:.....	9
3.1.5 Time of Flight (TOF).....	9
4. Verification: SCLC Mobility.....	12
4.1 Hole Only Device	12
5. Experiment and Results.....	13
5.1 Device Fabrication.....	13
5.2 Preliminary Measurements: IV, CV, Thickness, Series Resistance	14
5.3 Transient Photoconductivity Apparatus	17
5.4 SCLC Setup and Verification	19
6. Hybrid Devices	21
6.1 Preliminary Measurements	21
6.2 Transient Result.....	24
7. Experimental Error Calculation.....	28
8. Conclusion.....	29
9. Future Work.....	30
9.1 Correlation with PICTS.....	30
9.2 Correlation with Long-Pulse Transient Response	30
References	31

List of Figures and Tables

Figure 1. Record Solar Cell Efficiencies Since 1975. (Source: http://www.nrel.gov/ncpv/images/efficiency_chart.jpg)	1
Figure 2. Flexible organic solar cells. (Source: http://www.gizmag.com/world-record-efficiency-for-organic-photovoltaic-solar-cells/17186/picture/125812/)	2
Figure 3. A typical J-V curve of an Organic Solar Cell with its short circuit current (J_{sc}) and open circuit voltage (V_{oc}).	3
Figure 4. Difference between a bilayer and a bulk heterojunction architecture for P3HT:PCBM solar cells.....	4
Figure 5. The four steps of carrier transport in conjugated solar cells.....	5
Figure 6. Energy levels for a typical P3HT:PCBM device.	6
Figure 7. Space Charge Limited Current device architecture for (a) Hole-only device, and (b) Electron-only device.....	7
Figure 8. Device response to a linearly increasing voltage excitation in a CELIV setup. ...	8
Figure 9. A typical Time-of-Flight setup. The laser pulse creates charge carriers that travel across the thickness of the solar cell. The decay curve on the oscilloscope is used to extract the transit time.....	10
Table 1. Limitations on device structure and apparatus in order to measure mobility via transient photoconductivity and Space Charge Limited Current.....	12
Figure 10. Energy levels for a P3HT:PCBM hole-only device with an Au cathode.	13
Figure 11. The hole-only P3HT:PCBM device with a transparent ITO anode and Au cathode.....	14
Figure 12. Current-Voltage characteristics for the hole-only device (a) in the dark, and (b) in illumination.....	15
Figure 13. Capacitance-Voltage curve of the hole-only device. The peak capacitance indicates the built-in voltage.....	16
Figure 14. Series resistance of the hole-only device.....	16
Figure 15. Response of the laser diode and Agilent pulse generator setup. The rise time was less than 5ns.	17
Figure 16. Transient response of the hole-only device as seen on the oscilloscope.....	18

Figure 17. Double logarithmic plot for the hole-only device transient photocurrent response at -2V. The intersection of the linear fits gives the transit time.19

Figure 18. Semi-log J-V plot of the hole-only device in space charge regime. SCLC fit is found by using an appropriate value for mobility in the field-assisted SCLC equation. ..20

Table 2. Summary of mobility values for the hole-only device derived via Transient Photoconductivity and Space Charge Limited Current methods.....20

Table 3. P3HT:CdSe devices with four different ligands and their respective power conversion efficiencies.21

Figure 19. Dark Current-Voltage curves for (a) P3HT:CdSe(BA), (b) P3HT:CdSe(NL), (c) P3HT:CdSe(Py), and (d) P3HT:CdSe(tBT).22

Figure 20. Capacitance-Voltage curves for CdSe:P3HT(BA), CdSe:P3HT(NL), CdSe:P3HT(Py), and CdSe:P3HT(tBT). The peak capacitance indicates the built-in voltage.23

Figure 21. Series resistance for (a) CdSe:P3HT(BA), (b) CdSe:P3HT(NL), (c) CdSe:P3HT(Py), and (d) CdSe:P3HT(tBT).23

Table 4. Summary of active layer thickness and device built-in voltage for CdSe:P3HT(BA), CdSe:P3HT(NL), CdSe:P3HT(Py), and CdSe:P3HT(tBT). Thickness for CdSe:P3HT(NL) could not be determined accurately.24

Figure 22. Transient photocurrent response for (a) P3HT:CdSe(BA), (b) P3HT:CdSe(Py), and (c) P3HT:CdSe(tBT).....24

Figure 23. Double logarithmic plot for P3HT:CdSe(BA) at -3V. The intersecting linear fits give the transit time.....25

Figure 24. Double logarithmic plot for P3HT:CdSe(Py) at -3V. The intersecting linear fits give the transit time.....26

Figure 25. Double logarithmic plot for P3HT:CdSe(tBT) at -2V. The intersecting linear fits give the transit time.27

Table 5. Charge carrier mobilities for P3HT:CdSe(BA), P3HT:CdSe(Py), and P3HT:CdSe(tBT). Mobility for P3HT:CdSe(NL) could not be determined because its thickness could not be resolved.....27

Figure 26. Double logarithmic plots for three measurements of the hole-only P3HT:PCBM device.....28

Table 6. Calculated values of mobility from transients shown in Figure 26.....28

List of Symbols and Acronyms

Δj	Difference between maximum current and $j(0)$
ϵ	Relative permittivity
ϵ_0	Permittivity of free space
γ	Field-activation factor
v	Drift velocity
μ	Carrier mobility
μ_0	Zero-field mobility
ω	Angular frequency
AC	Alternating Current
Al	Aluminum
Au	Gold
BA	Butylamine
BHJ	Bulk heterojunction
C	Capacitance
CdSe	Cadmium Selenide
CELIV	Charge extraction by linearly increasing voltage
d	Device thickness
D/A	Donor/Acceptor
DC	Direct Current
DI	Deionized
E	Electric field
eV	electron volt
FF	Fill factor
G	Conductance
HOMO	Highest occupied molecular orbital
I, i	Current
Im	Imaginary
ITO	Indium tin oxide
J	Current density
$j(0)$	Initial step current
J_{sc}	Short-circuit current density
LUMO	Lowest unoccupied molecular orbital
NL	Native ligand

OFET	Organic field-effect transistor
OLED	Organic light-emitting diode
OPV	Organic Photovoltaic
P3HT	Poly (3-hexylthiophene)
PCBM, PC ₆₁ BM	[6,6]-phenyl C61-butyric acid methylester
PCE	Power conversion efficiency
PEDOT, PEDOT:PSS	Poly(3,4-ethylenedioxythiophene) Polystyrene sulfonate
PICTS	Photo-Induced Current Transient Spectroscopy
PTFE	Polytetrafluoroethylene
PV	Photovoltaic
PVDF	Polyvinylidene difluoride
Py	Pyridine
q, q_{photo}	Generated photocurrent
R	Resistance
Re	Real
rpm	Rotations per minute
SCLC	Space charge limited current
tBT	tert-butylthiol
TOF	Time-of-flight
t_{tr}	Transit time
UV	Ultraviolet
V	Voltage
V_a	Applied voltage
V_{bi}	Built-in voltage
V_{oc}	Open-circuit voltage
Y	Admittance

1. Introduction and Motivation

Over the past few decades, there has been a lot of interest in exploring alternative and renewable sources of energy to address the growing concern about environment and climate. Particularly, the discovery of climate change, owing to anthropomorphic activities leading to increased carbon emissions has caused people to think outside the box and find ways to produce and consume energy with a smaller and more sustainable carbon footprint [1]. Sustainable energy is the need of the hour. Amongst the various renewable energy generation options such as wind, biomass etc., Photovoltaic Energy generation is at the forefront and is expected to become very widespread and relevant in the near future [2]. However, solar energy has a long way to go before it becomes scalable and achieves grid parity [3]. This is essential for it to compete with traditional fossil fuel based energy systems, which have a higher energy density, and less cost per kilowatt. The next generation of solar cells needs to be more efficient and cost less.

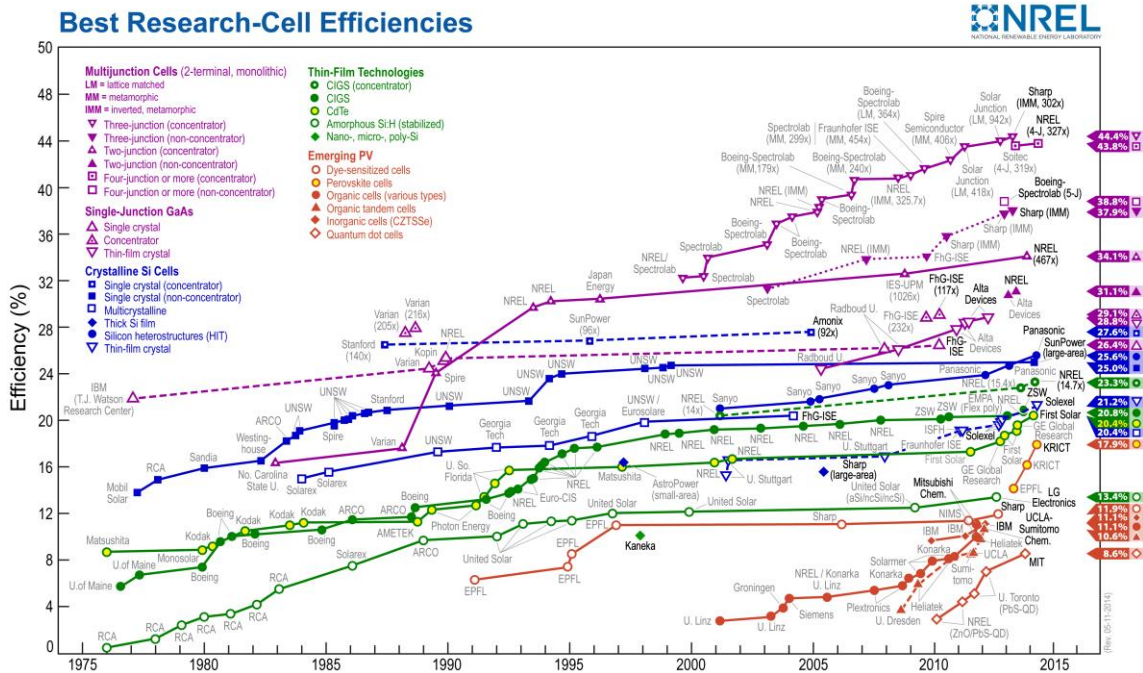


Figure 1. Record Solar Cell Efficiencies Since 1975. (Source: http://www.nrel.gov/ncpv/images/efficiency_chart.jpg)

Organic Photovoltaic (OPV) devices are the newest entry into the world of solar cells. Over the past two decades, there has been a lot of research on disordered semiconductors. The best organic solar cells today have an efficiency of up to 11% [4]. As shown in Figure 1, there has been an exponential rise in efficiency since the first organic solar cell was invented. While the efficiency of organic solar

cells is still much lower than their inorganic counterparts, researchers continue to show a lot of interest due to the low cost of flexible substrates that can be used for deposition of organic films and applications for which thin films are most appropriate [5]. Organics can be used in niche applications to supplement inorganic PVs as we move toward a more sustainable energy approach and try to integrate various renewable technologies. The flexible substrate also allows for roll-to-roll process printing, which has already been demonstrated by a few companies as a large-scale cost-effective production method [6]. Organic solar cells, therefore, have the potential to be very inexpensive to produce, as they do not demand expensive high purity inorganic crystals or high-temperature fabrication methods. However, before OPVs become competitive with inorganic solar cells, they need a lot more research to lower their cost and improve efficiencies [5,6].

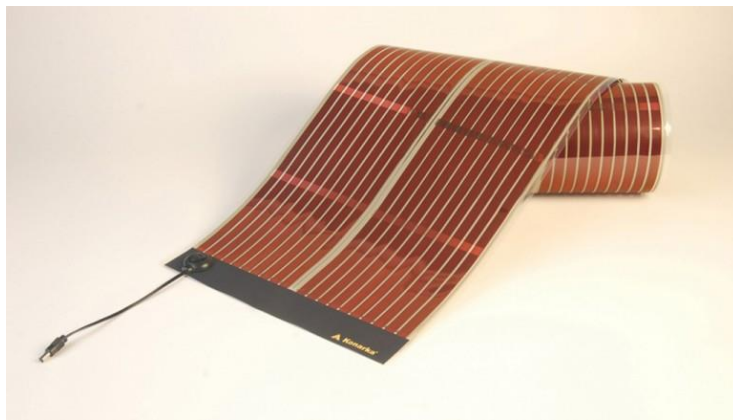


Figure 2. Flexible organic solar cells. (Source: <http://www.gizmag.com/world-record-efficiency-for-organic-photovoltaic-solar-cells/17186/picture/125812/>)

P3HT:PC₆₁BM (addressed as P3HT:PCBM from here on for simplicity) refers to a common type of blend used in organic solar cells. It consists of a polymer donor, poly (3-hexylthiophene) (P3HT) mixed with a fullerene acceptor, [6,6]-phenyl C₆₁-butyric acid methylester (PCBM). The best P3HT:PCBM solar cells have achieved efficiencies of > 5% [7,8]. Their electro-optic properties, low cost, and easy fabrication techniques make P3HT:PCBM devices ideal to compete with inorganic solar cells in the future [8]. However, many of the mechanisms that contribute to the physics of these organic solar cells are still unknown. Understanding the primary physical mechanisms in more detail is essential to enhancing their efficiencies. In this thesis I demonstrate a technique to measure the mobility of P3HT:PCBM and other organic and hybrid devices through transient photoconductivity.

2. Device Physics of Organic Solar Cells

2.1 Inorganic PN Junction

Inorganic solar cells are based on an n-type and a p-type semiconductor PN junction. The incoming light excites electrons from the valence band to the conduction band of the material, forming an electron-hole pair. In the vicinity of the depletion region, the electron-hole pair gets swept away in opposite directions by the built-in field and extracted by the electrodes into the external circuit. The PN junction can also be realized using two different materials, creating a heterojunction [9].

2.2 Organic Solar Cells

An organic solar cell uses disordered carbon-based molecules that have demonstrated photoconductive properties to convert photons into charge. The charge travels through the device to reach its electrodes resulting in current [5]. There are some important differences between the mechanisms of organic and inorganic solar cells.

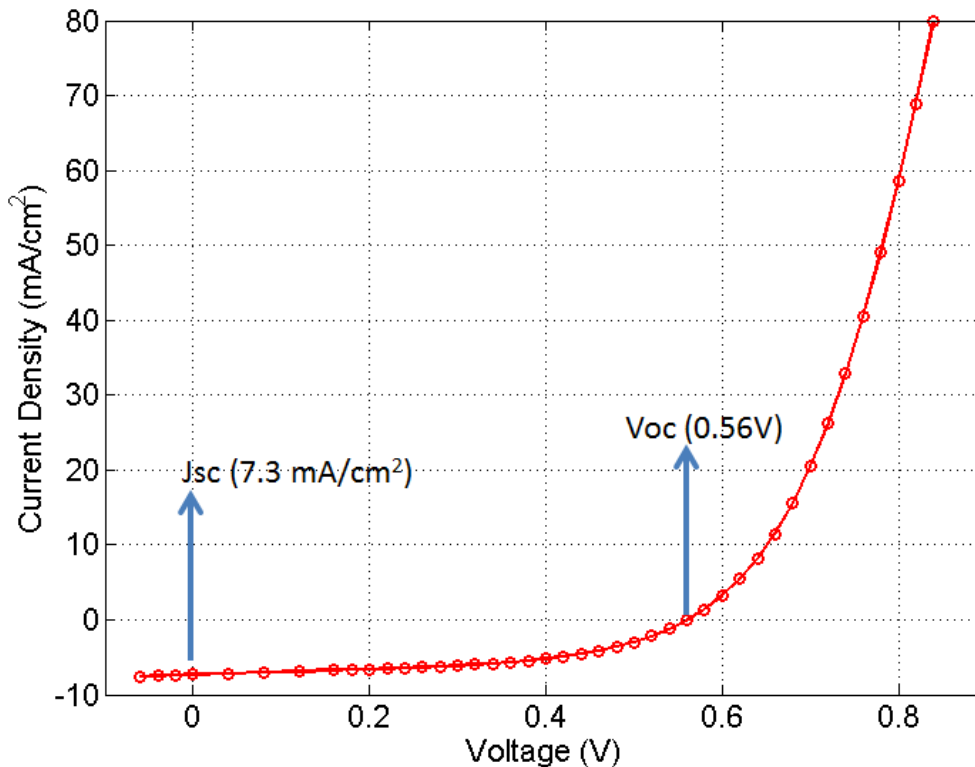


Figure 3. A typical J-V curve of an Organic Solar Cell with its short circuit current (J_{sc}) and open circuit voltage (V_{oc}).

2.2.1 Bilayer vs Bulk Heterojunction

A typical organic solar cell architecture is shown below. It contains the photosensitive active layer, which is a combination of a donor and an acceptor material. These materials consist of molecules and polymers that form conjugated systems via covalent carbon bonds that result in delocalized electrons in their π orbitals. These π electrons belong to a group of atoms instead of being tied to a single atom or bond. The “bandgap” of an organic semiconductor arises out of the energy difference between its two molecular π bands: the Highest Occupied Molecular Orbital (HOMO) and the Lowest Unoccupied Molecular Orbital (LUMO) levels. The incoming photons need to have enough energy to excite an electron from the HOMO level to the LUMO level to form an electron-hole pair. When placed under light, the donor, frequently P3HT, absorbs the incoming light and donates an electron to the acceptor, PCBM, leaving a hole state. However, transport of the electrons and holes to their respective electrodes is more complicated than in inorganic materials. Unlike crystalline solids, the electrons are still localized in the inter-molecular scale across the organic material. The electrons, therefore, have to hop from one π -system to the next with a certain transition probability. This “hopping mechanism” constitutes charge transport in organic materials [5]. For P3HT:PCBM solar cells, aluminum is typically used as the cathode to collect electrons, while a hole transport layer (HTL) of PEDOT:PSS is used to transport the holes to a transparent anode, typically Indium Tin Oxide (ITO) [7,10]. The P3HT:PCBM heterojunction can be designed in two different architectures, (i) bi-layer heterojunction, and (ii) bulk heterojunction, as shown in the Figure 4 [11].

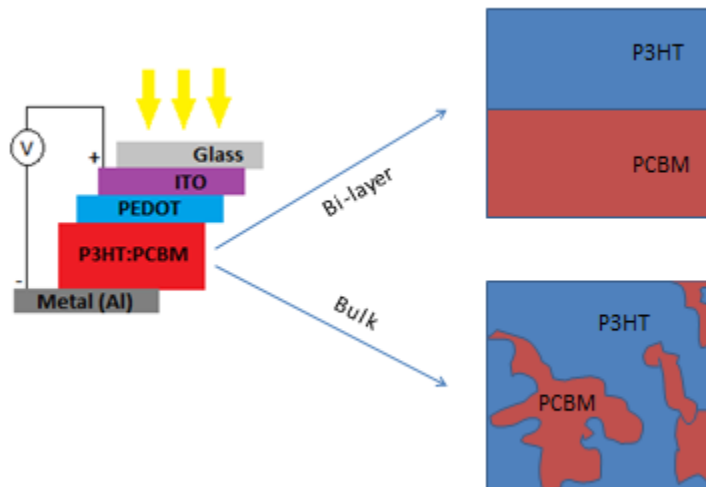


Figure 4. Difference between a bilayer and a bulk heterojunction architecture for P3HT:PCBM solar cells.

In a bilayer design, the donor and acceptor are stacked on top of one another, forming an effective Donor-Acceptor (D/A) interface, equivalent to a PN junction through the middle of the active layer. The early years of organic solar cells utilized this architecture. In contrast, the more modern architecture of a bulk heterojunction (BHJ) solar cell involves blending both the acceptor and donor molecules throughout the thickness of the film to provide a D/A interface that is spread throughout the organic blend [11]. The reason a BHJ architecture is preferred over a bilayer lies in understanding the functionality of organic solar cells. In a P3HT:PCBM solar cell carrier transport occurs in four steps:

Step 1: The P3HT donor molecule absorbs light to form a strong coulomb-bound exciton. These excitons have a very small recombination time and they need to get to a donor-acceptor interface to find a favorable energy state in order to split.

Step 2: The exciton pair diffuses to a D/A interface before recombining.

Step 3: The exciton pair donates an electron to the acceptor (PCBM) to form a polaron pair. However, this polaron pair is still weakly coulomb-bound and is not yet free to travel as free electrons and holes.

Step 4: With adequate built-in and/or applied field, the polar pair overcomes its coulomb attractive forces forming free electron and hole polarons. In this work we will simply refer to these as electrons and holes analogous to transport in inorganics [12].

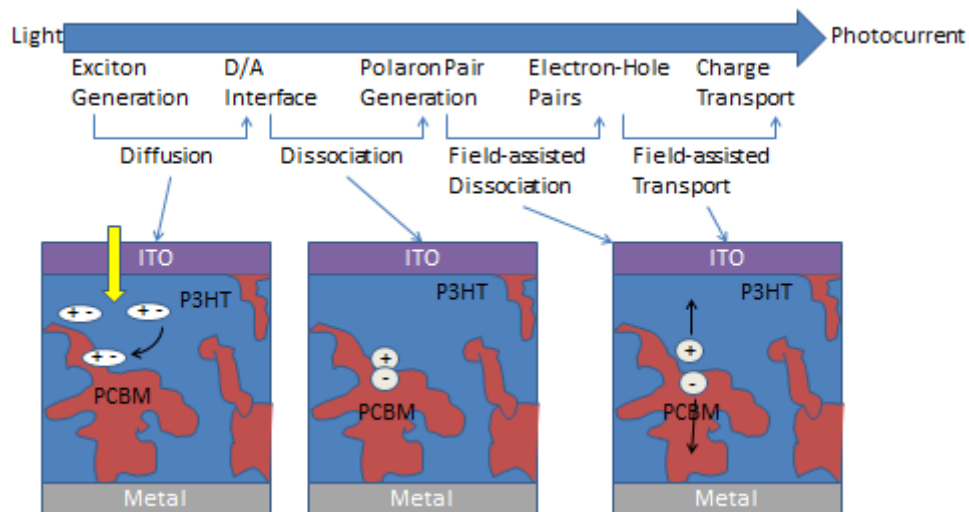


Figure 5. The four steps of carrier transport in conjugated solar cells.

The electrons and holes then travel in opposite directions as directed by the field to reach the respective electrodes. The problem with bilayer organic solar cells

is that very few of the excitons make it to the D/A Interface prior to recombining. It is mainly the photons that fall in the immediate vicinity of the bilayer junction that produce free charge carriers. The very low exciton recombination time prevents exciton pairs generated elsewhere to successfully proceed to free carrier transport. Since organic solar cells are thin ($\sim 100\text{nm}$) to begin with, the PN region of bi-layer structures is extremely thin resulting in very poor efficiencies [11]. With a BHJ architecture, the device circumvents the problem by providing a distributed networks of D/A interfaces, which, in turn, provides excitons more chances to find a favorable energy state to separate into bound polarons, and then into free carriers. The merits of a BHJ architecture are evident in the higher Power Conversion Efficiencies (PCE) that they have achieved. A good BHJ architecture requires blending P3HT and PCBM molecules in controlled conditions to provide ideal morphology and phase separation to ensure that the excitons find enough D/A interface states, and yet not impede the carrier flow through the acceptor and donor channels towards the respective electrodes [11,12].

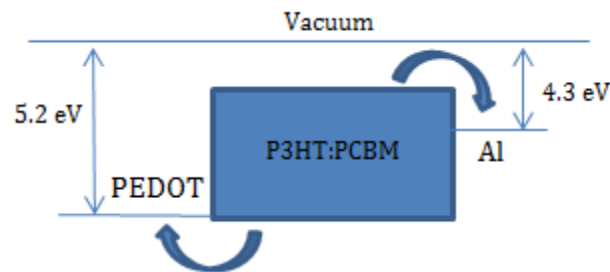


Figure 6. Energy levels for a typical P3HT:PCBM device.

3. Carrier Mobility

Carrier mobility is an indication of how fast the carriers (electrons and/or holes) can move through a semiconductor under the influence of an electric field [9]. The higher the mobility, the less time carriers take to reach their electrodes and generate current. Mobility has been explored and studied thoroughly in inorganic solar cells [13,14]. However, there is still a lot to learn about what governs mobility in organic and hybrid solar cells. Learning about and improving mobility in organic cells translates into increased efficiency [15]. Further, having a direct and easy-to-implement technique would help to reduce the cost and time in characterizing organic solar cells. Typically in inorganic semiconductors, mobility is measured using the “Hall Effect”, which is based on measuring the deviation of electrons under the influence of a magnetic field. A Hall Effect machine is quite common for characterizing inorganic solar cells and semiconductors. However, Hall Effect machines are limited to materials with mobilities of $1\text{cm}^2/\text{V}\cdot\text{s}$ and above [16,17]. Organic solar cells display mobilities far lower than that. Hence, we have to rely upon alternative techniques to find mobility in such disordered materials.

3.1 Mobility Measurements in OPVs

Carrier mobilities in organic semiconductors are approximately a 1000 times less than those in typical Si solar cells [15]. The transport mechanism of carriers in OPVs, organic light-emitting diodes (OLEDs), and organic field-effect transistors (OFETs) relies upon a hopping mechanism through favorable energetic sites, as opposed to the free pathways available to electrons and holes in inorganic semiconductors. This limits the mobility of the device and also requires different measurement techniques. To date, a few techniques to measure mobility in thin film devices have been reported [18,19]. These are briefly described below. Of these, time of flight offers the most direct method of measurement.

3.1.1 Space Charge Limited Current (SCLC):

The SCLC technique requires an ohmic electrode for charge injection at one end and a blocking contact on the other end to maintain a single carrier regime.

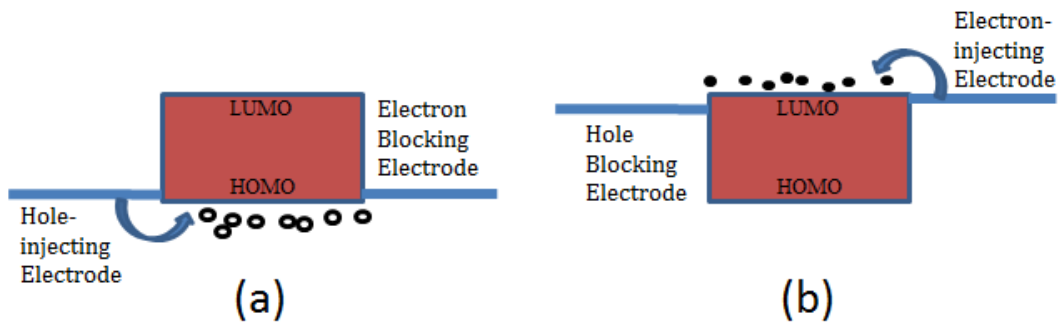


Figure 7. Space Charge Limited Current device architecture for (a) Hole-only device, and (b) Electron-only device.

At high voltages, the device enters a space charge regime and the injected carrier travels through the device with a mobility that can be derived using the J-V relationship established by Mott-Gurney:

$$J = \frac{9}{8} \cdot \mu \cdot \epsilon \cdot \epsilon_0 \cdot \frac{V^2}{d^3},$$

where J is the current density, V is the applied voltage, μ is the mobility, ϵ is the dielectric constant, ϵ_0 is the permittivity of free space, and d is the device thickness.

If the material shows field and temperature dependence of mobility, the equation is modified to:

$$J = \left(\frac{9}{8}\right) \cdot \varepsilon \cdot \varepsilon_0 \cdot \mu_0 \cdot \exp\left(0.891\gamma \cdot \sqrt{\frac{V}{d}}\right) \cdot \frac{V^2}{d^3},$$

where μ_0 is the zero-field mobility and γ is the field activation factor. The higher the value of gamma, the more dependent mobility is on the electric field. By carefully choosing electrodes with the required work functions to guarantee an SCLC regime, the solar device can be probed for dark J-V characteristics. Using the SCLC equations above, the best fit provides the mobility [19].

3.1.2 Charge Extraction by Linearly Increasing Voltage (CELIV)

In the CELIV setup, a linearly increasing voltage pulse of width t_{pulse} with a slope of $A = V/t_{\text{pulse}}$ is applied to a device for a short duration to generate a current transient response.

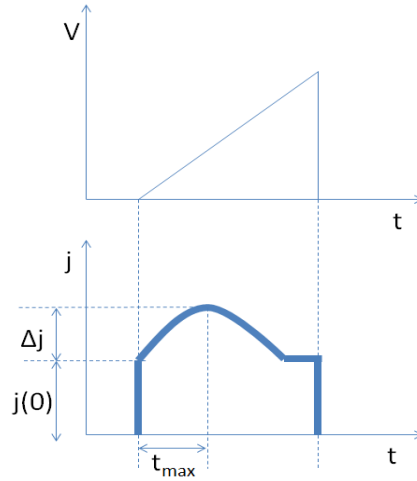


Figure 8. Device response to a linearly increasing voltage excitation in a CELIV setup.

First, an initial step response is observed due to the capacitance of the device, which can be described by the equation:

$$j(0) = \frac{\varepsilon \cdot \varepsilon_0 \cdot A}{d}$$

The current response increases due to extraction of dominant charge carriers until it reaches a peak before decreasing. The position of this peak is defined as t_{\max} and is used to calculate mobility using the equation;

$$\mu = \frac{2d^2}{3A \cdot t_{\max}^2} \cdot \left(1 + 0.36 \frac{\Delta j}{j(0)} \right)^{-1}$$

where A is the slope and Δj is the difference between $j(0)$ and the maximum current [18,19].

3.1.3 Impedance Spectroscopy

Impedance spectroscopy uses the device AC response to extract mobility. It requires the sample to have the same geometry as that for SCLC. The sample is injected with a DC bias to achieve the space charge regime. A small AC voltage is also applied and the AC current response is studied. The sample admittance, $Y = I_{ac}/V_{ac}$ exhibits a frequency dependence. Therefore, the sample conductance $G = \text{Re}\{Y\}$ and capacitance $C = \text{Im}\{Y/\omega\}$ also shows a frequency dependence. When G and C are plotted against the AC frequency, the spectra displays a decrease in G and increase in C at the frequency $\omega = 1/t_{tr}$, where t_{tr} is the carrier transit time. Using the following equation one can extract the mobility [19]:

$$t_{tr} = \frac{4d^2}{3\mu \cdot V_{dc}}$$

3.1.4 Transient Photoconductivity:

Transient photoconductivity is a common technique that employs analysis of photocurrent decay. Unlike the previous three methods, transient photoconductivity relies upon photon excitation of the device under study. Typically, a laser pulse shines light on the sample and produces a photocurrent pulse. The pulse then decays as the generated carriers either make their way to the electrode or recombine. Therefore, transient photoconductivity is a good tool to study sweep-out and recombination kinetics in low mobility materials [20,21]. The decay time and shape provides vital information about the device properties.

3.1.5 Time of Flight (TOF)

Time of Flight (TOF) uses a transient photoconductivity setup under specific conditions to derive the carrier mobility. While TOF does not require an ohmic contact for any of its electrodes, it does require one transparent contact (such as ITO) to shine the light through, and a device thickness that exceeds $1\mu\text{m}$ in order to

reduce the device capacitance, and minimize RC response effects on the shape of the transient. It is also important that the light is absorbed in a thin localized sheet close to one electrode. Under the influence of an applied field, the generated carriers then travel from one electrode across the length of the device to the other electrode. After each light pulse, the resulting photocurrent pulse decays as it progresses to the other electrode. This “transit” time (t_{tr}) can be extracted from the transient decay curve. When the carriers reach the electrode, the decay curve shows a distinct plateau, which indicates the transit time. However, disordered semiconductor materials such as P3HT:PCBM can be dispersive in nature, and their transient decay curve shows no kink. This is due to the presence of traps at various energy levels [19]. In such cases, a log-log plot of the decay curve is used and the linear fits to the log-slopes yield the transit time.

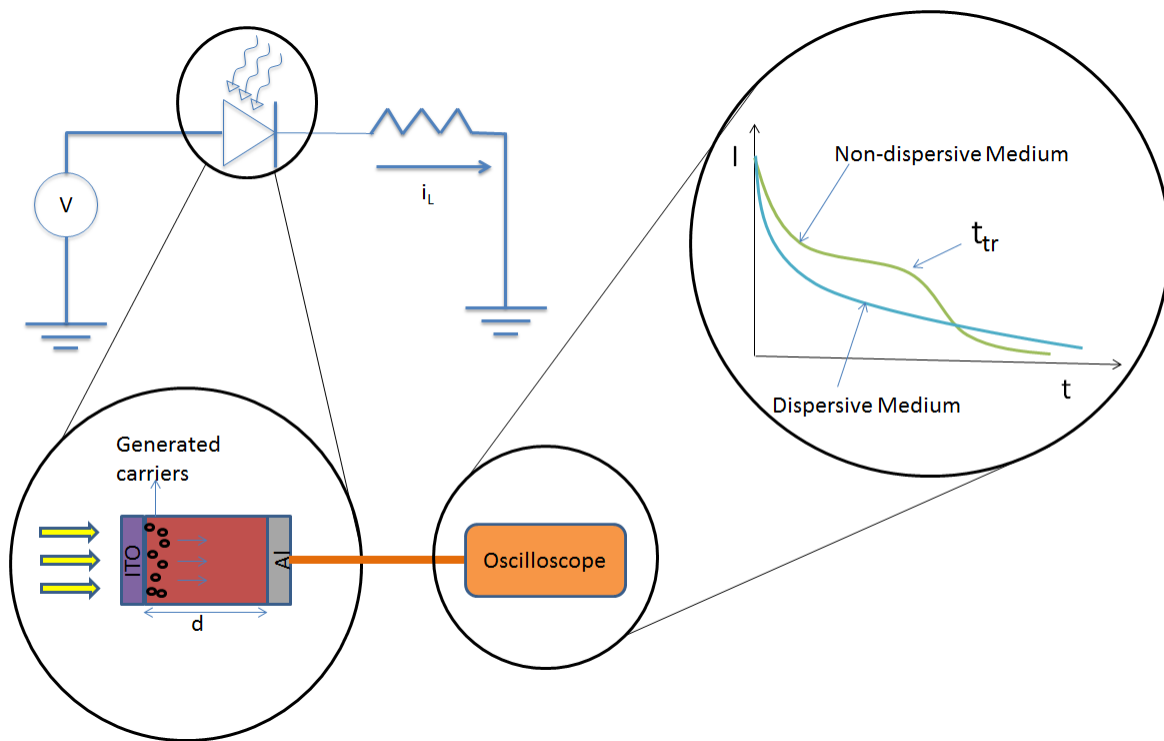


Figure 9. A typical Time-of-Flight setup. The laser pulse creates charge carriers that travel across the thickness of the solar cell. The decay curve on the oscilloscope is used to extract the transit time.

The photocurrent is primarily drift current with negligible contributions from diffusion current. At high internal fields, most of the charge is transported to the electrodes, and there is little recombination. In such a regime, the transit time is given by the device thickness divided by the carrier drift velocity:

$$t_{tr} = \frac{d}{v},$$

where d is the device thickness, v is the drift velocity, and t_{tr} is the transit time. The drift velocity is well established by the equation:

$$v = \mu \cdot E = \mu \cdot \frac{V}{d},$$

where μ is the charge carrier mobility and E is the internal electric field. This yields an equation for the mobility in terms of the device thickness and transit time:

$$\mu = \frac{d^2}{V \cdot t_{tr}}.$$

Each method described above imposes restrictions on the device architecture and/or the device setup. While SCLC and impedance spectroscopy are straightforward methods, they require deposition of a blocking contact to make the device a single-carrier semiconductor [19]. This method is viable if the devices can be fabricated and characterized under identical conditions. Regular P3HT:PCBM and other thin-film organic/hybrid solar cells use injecting electrodes on both ends. To characterize such a device, especially one that might have been fabricated elsewhere, TOF and CELIV are the better alternatives. Of the two, TOF is the most direct and simple procedure to find mobility. However, owing to the thin-film nature of BHJ solar cells, researchers have avoided this technique [18,19]. In this thesis, I successfully extract carrier mobility of a P3HT:PCBM BHJ solar cell through a modified transient photoconductivity analysis, and verify the result via SCLC.

3.1.5.1 TOF in Thin Film Organic Solar Cells

To perform any transient photocurrent decay analysis, the first limitation that has to be kept in mind is that the device response, in the form of its RC time constant, must be smaller than the decay response that one is trying to measure. In this case, the device RC time constant should be smaller than the transit time of the charge carriers. Traditional TOF analysis also requires that the photo-induced charge be much less than the field-induced charge ($q_{photo} \ll CV$) in order to not distort the otherwise uniform electric field under which the carriers travel. However, the charge should be large enough to generate a signal which is visible on the oscilloscope and can be separated from noise. The third limitation that must be considered is that the dielectric relaxation time should be much larger than the transit time (i.e. the time between the pulses should be \gg pulse width) to allow the device to relax back to its equilibrium state before being subjected to photo-excitation [19].

Since the active layer thickness in a P3HT:PCBM solar cell is approximately 100nm, it is hard to perform TOF analysis on it. A very thin film has a high RC time constant which prevents the necessary resolution required to study the decay tail. Furthermore, the photocurrent is generated throughout the device thickness instead of in a thin localized region. However, with some minor tweaking it is possible to

perform a valid transient photoconductivity analysis on these 100 nm-thick devices and derive mobility from them. Cowan et al. have successfully applied the TOF technique by using a transient photoconductivity method to determine mobilities for P3HT:PCBM devices using the formula:

$$\mu = \frac{d^2}{[2 \cdot (V_a + V_{bi}) \cdot t_{tr}]}$$

The factor of 2 is included since the device thickness is extremely small, resulting in carrier generation throughout the active area. Thus, the carriers travel approximately half the distance [21]. If the device thickness were on the order of microns, the factor of 2 would be omitted. Cowan et al. used a low resistance setup to ensure that the RC time constant is less than the transit times. In this thesis, I use and verify Cowan’s method and formula to find mobility in P3HT:PCBM solar cells.

4. Verification: SCLC Mobility

To verify the mobility derived from transient photoconductivity, I decided to use SCLC due to its well-established and simple technique. It was also necessary to use a method that was not constrained by device thickness to address any concerns about the thin film limitations on photocurrent transients. Therefore, I decided to measure the mobility of the same device via SCLC and compare it to the result obtained via transient photoconductivity. This meant fabricating a device with one ohmic contact and one blocking contact. Such a device satisfies requirements for both SCLC as well as transient photoconductivity.

Methodology	Limitations
Transient Photoconductivity	$RC < t_{tr}$, $q \ll CV$, $t_{pulse} \ll$ Dielectric Relaxation time
SCLC	1 Ohmic injecting contact, 1 blocking contact (single carrier device)

Table 1. Limitations on device structure and apparatus in order to measure mobility via transient photoconductivity and Space Charge Limited Current.

4.1 Hole Only Device

To prepare a single-carrier device I chose a hole-only device architecture. This architecture ensures hole transport while electrons are blocked. This is

accomplished by depositing Au instead of Al as the cathode. The device architecture is as follows: ITO:PEDOT:P3HT:PCBM:Au.

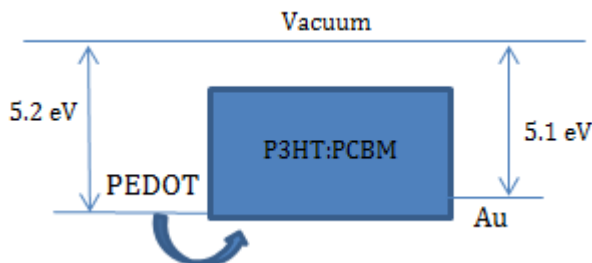


Figure 10. Energy levels for a P3HT:PCBM hole-only device with an Au cathode.

The work function of Au is much larger than that of Al, which results in the aligning of the Fermi level closer to the HOMO level of PCBM. This architecture has been used by many and has been cited in the past [22-24]. A positive bias on the ITO pushes the holes into the device where they are efficiently transported through the PEDOT. On the other side, even with a negative bias on Au, electron injection is blocked due to the work function gap between the Au Fermi level and the P3HT LUMO level.

It is important to note that even an SCLC fit to an IV curve of a conventional P3HT:PCBM structure with electrodes that enable both hole and electron injection (such as ITO:PEDOT:P3HT:PCBM:Al) would be physically meaningless, even if it provides seemingly correct mobility values, because the regime is never limited by a space charge build-up if both carriers are injected [25]. Therefore, it was necessary to fabricate and test the transient mobility of a P3HT:PCBM device with gold as the cathode to suppress electron injection. The larger work function of gold means that there is not much difference between the ITO and Au electrode work functions. This leads to a smaller built-in voltage. Therefore, while charge separation due to a smaller V_{bi} prevents this design from being an ideal organic solar cell, its physical nature at high forward and reverse biases (required for SCLC and Transient Photoconductivity, respectively) remains the same.

5. Experiment and Results

5.1 Device Fabrication

The P3HT and PCBM powders were purchased from Sigma Aldrich and were stored in a vacuum desiccator in the dark. To prepare the solution, 20 mg of P3HT was dissolved in 1 ml of Chlorobenzene and 18 mg of PCBM was dissolved in 1 ml of Chlorobenzene. The two solutions were kept on a magnetic stirrer for 12 hours.

After 12 hours, the two solutions were mixed in a 1:1 ratio and kept on the same stirrer for another 12 hours.

The solution was then ready to be spin coated on the substrate. The substrate was a glass film coated with ITO. The substrate was first treated with oxygen plasma to get rid of any surface impurities. Then, it was cleaned by dipping it into acetone in an ultrasonic container for 5 minutes, and then in ethanol in ultrasonic for another 5 minutes. The substrate was then rinsed with DI water and blow dried with nitrogen. In the next step, a PEDOT solution was cast on the clean substrate and spin coated at 4000 rpm for 40 seconds using a 0.2 micron PVDF filter. A smooth texture was ensured before moving on to the next step. The wafer was annealed in the dark and in vacuum at 120 degrees Celsius for 50 minutes. The P3HT:PCBM solution was cast upon the substrate using a PTFE filter and spin coated at 900 rpm for 1 minute. The wafer was then inserted in an electron-beam evaporator to deposit 100nm of Au as the cathode. The device was then annealed at 140 degrees Celsius for 30 minutes in vacuum and dark. The device was encapsulated by applying epoxy and treating it in a UV lamp for 3 minutes.

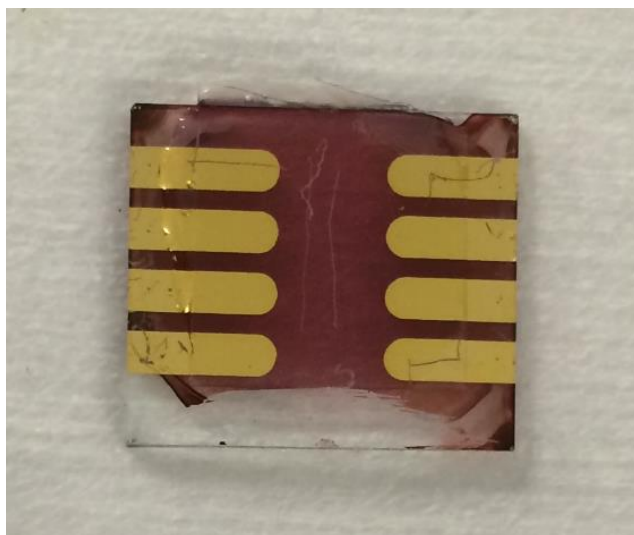


Figure 11. The hole-only P3HT:PCBM device with a transparent ITO anode and Au cathode.

5.2 Preliminary Measurements: IV, CV, Thickness, Series Resistance

Dark and Illuminated IV characteristics of the hole-only device were measured (Figure 12). The device yielded a short circuit current density (J_{sc}) of 4.5 mA/cm², an open-source voltage (V_{oc}) of 0.17 V, and fill factor (FF) of 0.29. The PCE was 0.21%. The low V_{oc} was expected due to the similar work functions of PEDOT and gold. The similar work functions also led to a small built-in voltage, which was responsible for inefficient charge separation and extraction, leading to low J_{sc} , and ultimately, to low PCE. However, the physics of charge extraction and charge injection in the bulk at high positive and negative bias stayed the same as

conventional P3HT:PCBM solar cells with Al contact. The dark IV curve was used to fit to the SCLC equation.

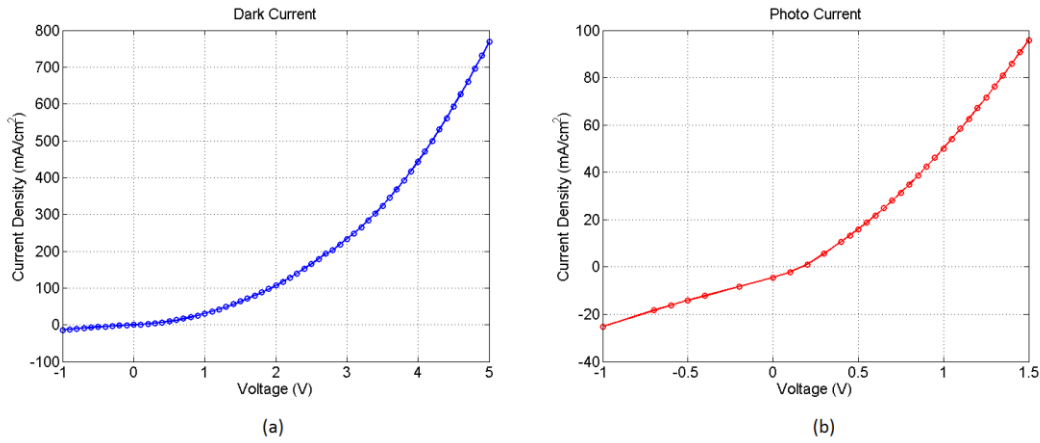


Figure 12. Current-Voltage characteristics for the hole-only device (a) in the dark, and (b) in illumination.

The capacitance of the device was also measured as a function of voltage (Figure 13). From negative bias to the positive built-in voltage, the capacitance is geometric and follows the Mott-Schottky relationship where the capacitance is inversely dependent upon the depletion region. The depletion region minimizes at the built-in voltage, resulting in the highest capacitance value. Therefore, the peak capacitance of the device can be used to estimate the built-in potential [26]. After reaching the peak, the device capacitance dips and switches predominantly to the chemical capacitance.

A built-in voltage of 0.2 V is derived from the CV curve, which is consistent with the difference in work function alignments of Au and PEDOT with the LUMO level of P3HT and the HOMO level of PCBM, respectively.

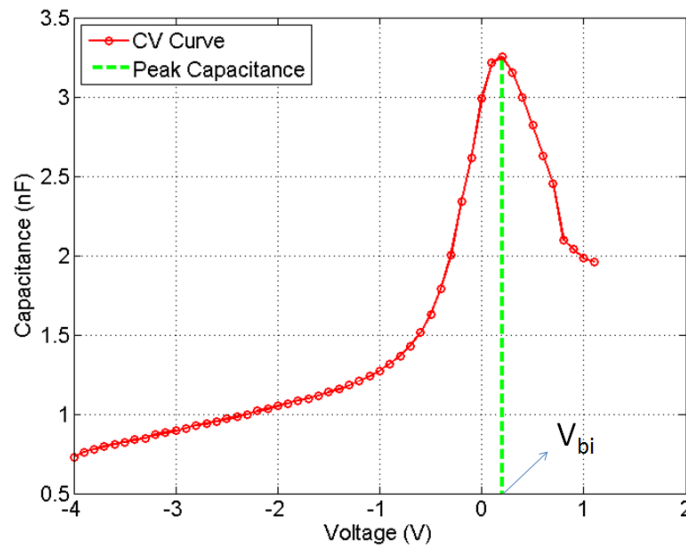


Figure 13. Capacitance-Voltage curve of the hole-only device. The peak capacitance indicates the built-in voltage.

The thickness of the active layer was determined to be 107 nm (+/- 5 nm) via a profilometer. First, the thickness of the PEDOT+P3HT:PCBM layer was measured; it was 167nm. Then, the thickness of a substrate with just PEDOT was measured. Its thickness was 60nm. The difference between the two layers provided the active layer thickness.

To find the device RC time constant, its series resistance was calculated from the IV characteristic using the relation $R = dV/di$ [27]. The series resistance of 25 ohms and the measured capacitance yielded a system RC time constant of 80 ns.

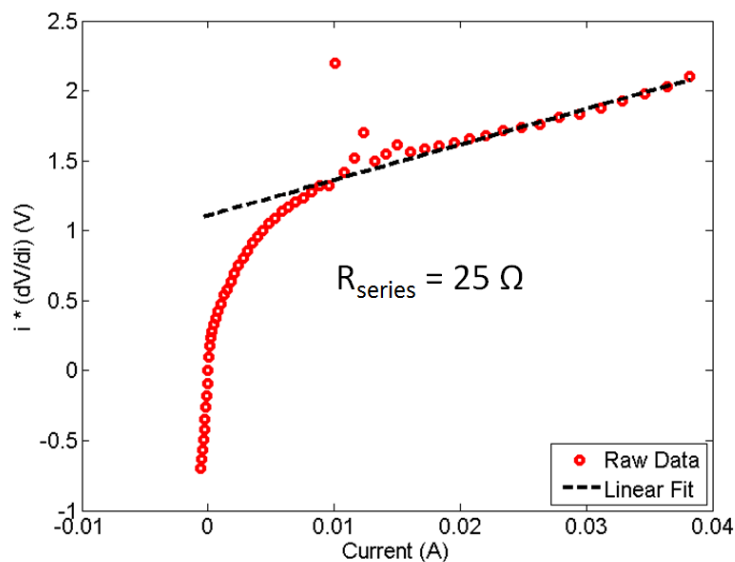


Figure 14. Series resistance of the hole-only device.

5.3 Transient Photoconductivity Apparatus

The transient photoconductivity setup consists of the hole-only device placed inside a probe station, with the probe tips in contact with the ITO and the Au electrodes. The device is held under a bias of -2 V DC using an HP pulse generator. The cathode of the device is connected to an Agilent high-speed oscilloscope with an impedance of 50 ohms in order to measure the photocurrent pulse. A 404 nm blue laser diode was used to excite the device with a 200 ns pulse. The laser diode was driven by an Agilent pulse generator. The measurement response was tested using a high-speed Hamamatsu PIN photodiode. It was found to be less than 5 ns. The response is shown below in Figure 15.

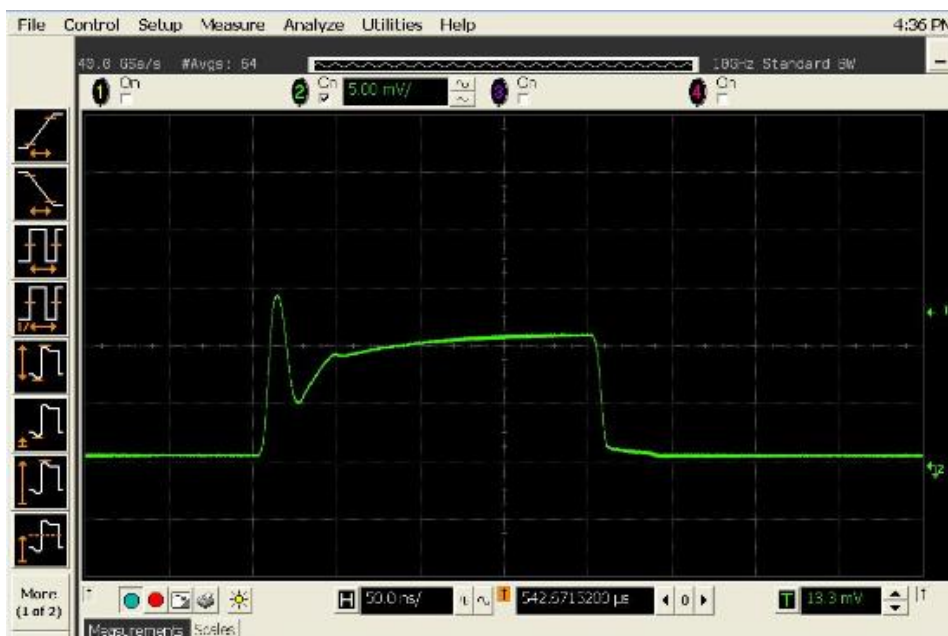


Figure 15. Response of the laser diode and Agilent pulse generator setup. The rise time was less than 5ns.

For measurements of the organic devices the pulse was repeated with a low frequency of 20 Hz to ensure abundant dielectric relaxation time. The signal is seen on the oscilloscope as a voltage pulse, which has a log tail indicative of dispersive transport [21]. The decay of the pulse gives the transit time. Since the signal is dispersive, its intersection is more visible on a log-log scale.

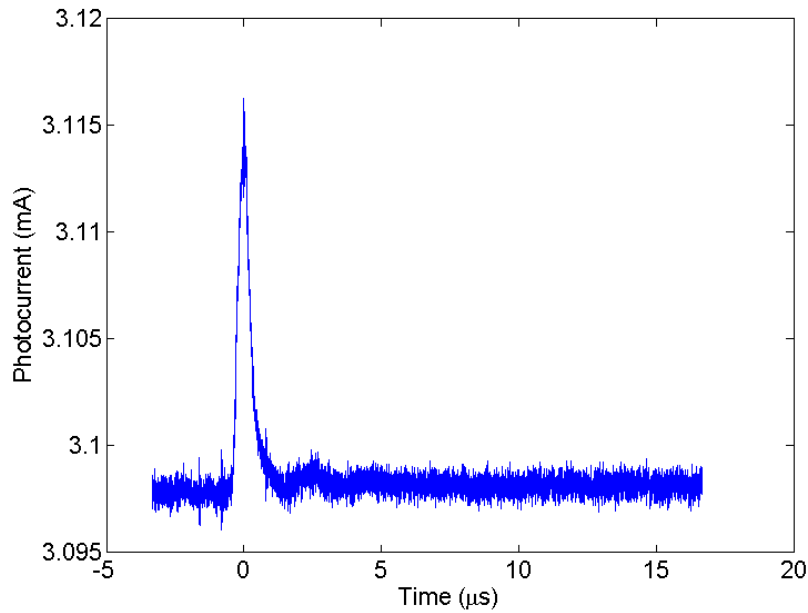


Figure 16. Transient response of the hole-only device as seen on the oscilloscope.

To confirm that the photo-induced charge does not alter the internal field, the total charge is calculated from the transient. By integrating the total photo pulse, we get the total charge induced inside the device due to photo-excitation, which is $\sim 8 \times 10^{-12}$ Coulombs. The charge due to the internal electric field is $q = CV$. The calculated capacitance at -2V DC is 1 nF and therefore the electric field charge is 2×10^{-9} C, which is much higher than the photo-charge. Hence, the transient pulse decays under the applied electric field.

In a log-log plot, the photocurrent shows a gradual decay with two linear, intersecting regions. When fitted with two linear fits, the intersection gives the transit time.

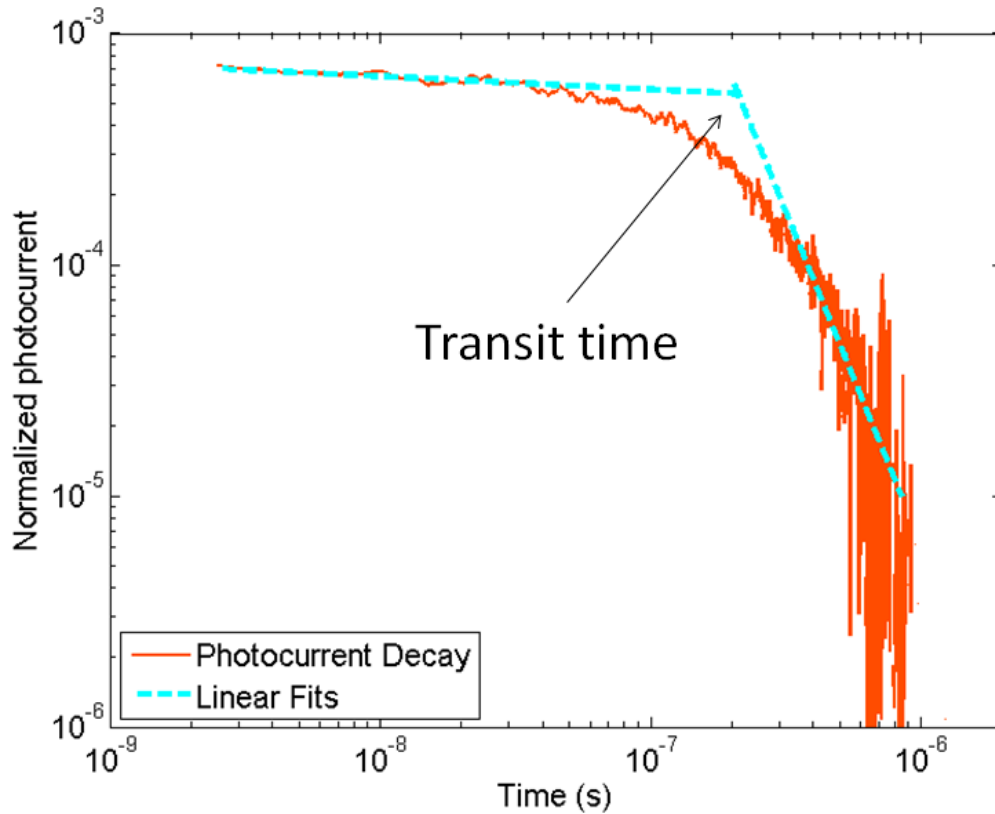


Figure 17. Double logarithmic plot for the hole-only device transient photocurrent response at -2V. The intersection of the linear fits gives the transit time.

The transit time, t_{tr} determined by this approach is ~ 210 ns. The device RC time constant was calculated to be 80 ns, which is less than t_{tr} . Therefore the device is not RC limited. Since, for a thickness of 107nm, in the visible range the P3HT:PCBM blend generates charges throughout its thickness, a factor of 2 is added in the denominator [21]. Therefore, I used the formula:

$$\mu = \frac{d^2}{[2 \cdot (V_{,a} + V_{,bi}) \cdot t_{,tr}]}$$

which produces a mobility of $1 \times 10^{-4} \text{ cm}^2/\text{V} \cdot \text{s}$.

5.4 SCLC Setup and Verification

For the SCLC setup the device is placed in an IV probe station. A Keithley source meter is used to supply voltage. The PEDOT injects holes, while the gold cathode blocks electron injection. At bias higher than the built-in voltage, the device enters the space charge regime [28]. The dark current is measured and mobility is extracted using the SCLC equation:

$$J = \left(\frac{9}{8}\right) \cdot \epsilon_0 \cdot \epsilon \cdot \mu \cdot \exp\left(0.891 \cdot \gamma \cdot \sqrt{\frac{V}{d}}\right) \cdot \frac{V^2}{d^3}$$

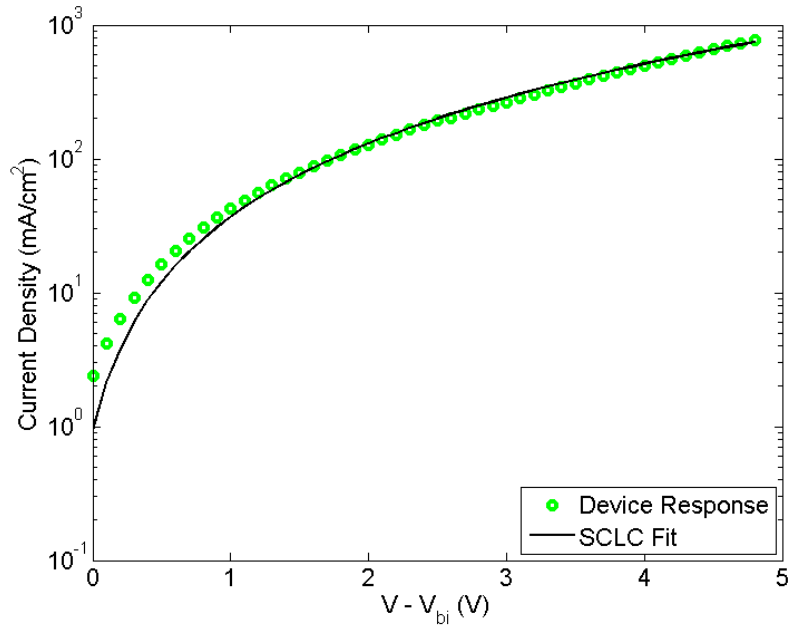


Figure 18. Semi-log J-V plot of the hole-only device in space charge regime. SCLC fit is found by using an appropriate value for mobility in the field-assisted SCLC equation.

After accounting for the built-in field, the fit to the dark IV data yields an SCLC mobility of $9 \times 10^{-5} \text{ cm}^2/\text{V.s}$. This value is very close to the one obtained by the transient photoconductivity method. Hence, this is proof of the robustness of the transient photoconductivity method for obtaining mobility for thin film solar cells.

Method	Mobility ($\text{cm}^2/\text{V.s}$)
Transient Photoconductivity	1×10^{-4}
SCLC	9×10^{-5}

Table 2. Summary of mobility values for the hole-only device derived via Transient Photoconductivity and Space Charge Limited Current methods.

6. Hybrid Devices

Once the technique of finding mobility via transient photoconductivity was verified, it was used to evaluate the mobility for three different P3HT:CdSe hybrid devices fabricated by Matt Greaney in Richard Brutchey's group at University of Southern California. P3HT:CdSe devices consist of a bulk heterojunction blend architecture that uses inorganic CdSe nanocrystal acceptors in combination with organic P3HT donors. Each acceptor molecule has a particular type of ligand.

For this experiment, P3HT:CdSe devices were chosen with four different ligands for comparison: Butylamine (BA), NL (Native Ligand), Pyridine (Py), and tert-butylthiol (tBT). Efficiencies of these devices were calculated at USC and are shown below.

Ligand	PCE
BA	1-1.5%
NL	0.3%
Py	2%
tBT	2.5%

Table 3. P3HT:CdSe devices with four different ligands and their respective power conversion efficiencies.

To understand if carrier mobility correlates with the efficiency values, transient photocurrent measurements were performed on these devices to derive their mobilities.

6.1 Preliminary Measurements

IV and CV curves for each device are shown in Figure 19 and Figure 20.

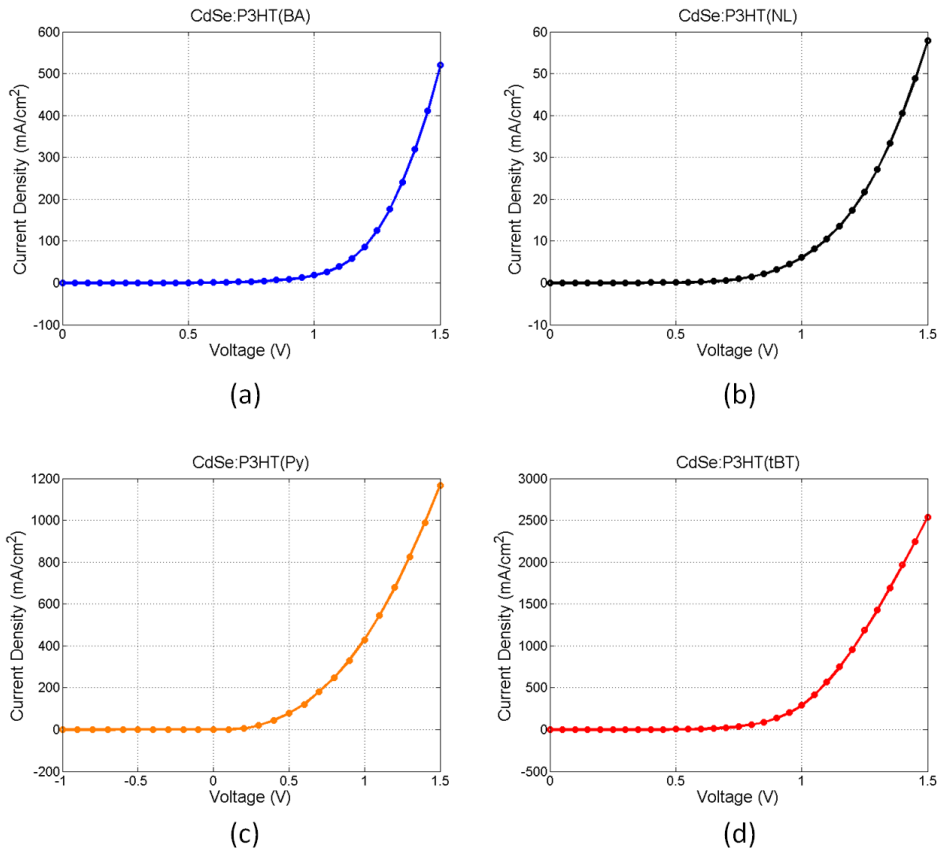


Figure 19. Dark Current-Voltage curves for (a) P3HT:CdSe(BA), (b) P3HT:CdSe(NL), (c) P3HT:CdSe(Py), and (d) P3HT:CdSe(tBT).

The IV curves were used to extract series resistance (Figure 21) and the CV curves were used to determine the built-in voltage and capacitance values, to be used for RC time constant calculations.

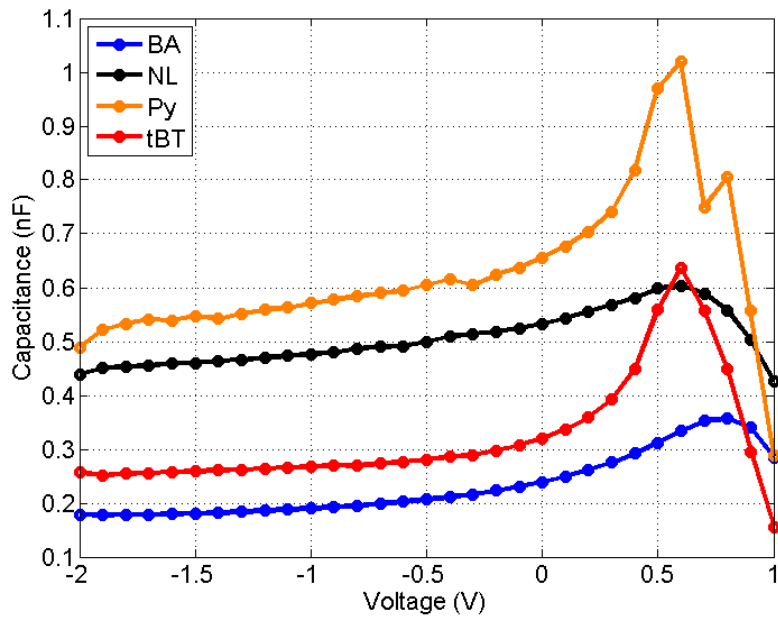


Figure 20. Capacitance-Voltage curves for CdSe:P3HT(BA), CdSe:P3HT(NL), CdSe:P3HT(Py), and CdSe:P3HT(tBT). The peak capacitance indicates the built-in voltage.

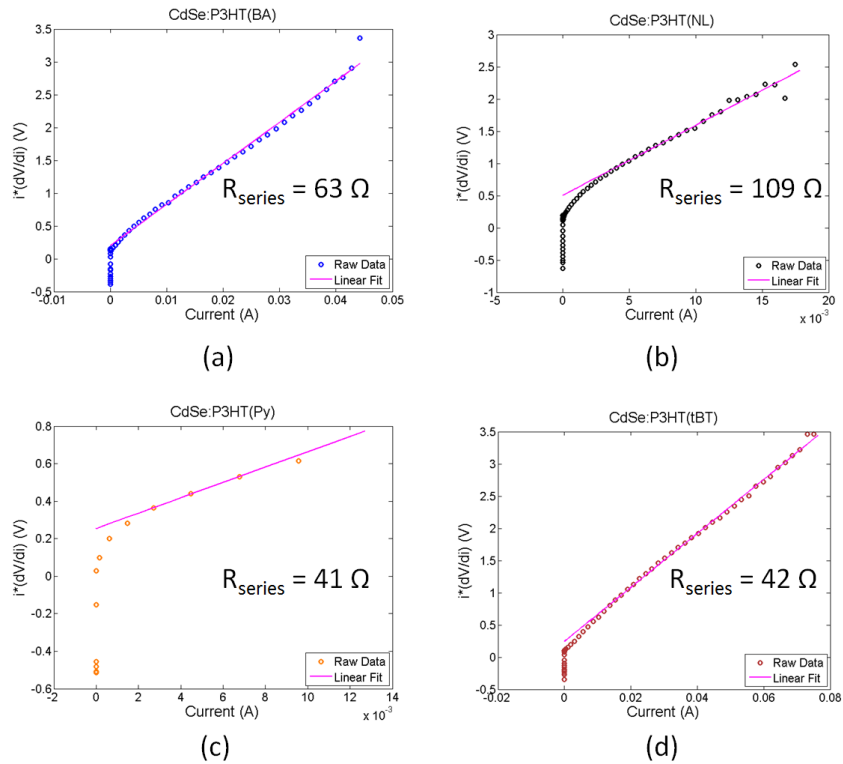


Figure 21. Series resistance for (a) CdSe:P3HT(BA), (b) CdSe:P3HT(NL), (c) CdSe:P3HT(Py), and (d) CdSe:P3HT(tBT).

The devices were placed in a profilometer to measure their thickness. A separate sample with just PEDOT was fabricated to extract the PEDOT thickness. This value was then used to determine the total active layer thickness. This is the thickness that electrons and holes have to travel in response to a photocurrent pulse in the transient setup. The thickness of NL could not be determined as the surface was uneven and there was large variation in the profilometer measurements. Thus, NL was not used for further calculations. A summary of the built-in voltage and thickness are shown below:

Ligand	Thickness (nm)	Built-In Voltage (V)
BA	68	0.8
NL	?	0.6
Py	65	0.6
tBT	65	0.6

Table 4. Summary of active layer thickness and device built-in voltage for CdSe:P3HT(BA), CdSe:P3HT(NL), CdSe:P3HT(Py), and CdSe:P3HT(tBT). Thickness for CdSe:P3HT(NL) could not be determined accurately.

6.2 Transient Result

The same setup was used as for the P3HT:PCBM device. The only difference was that the laser diode intensity was increased in order to obtain measurable photocurrent. The induced charge is still much less than the CV product for each device. The transient decay curves are shown for the three ligands.

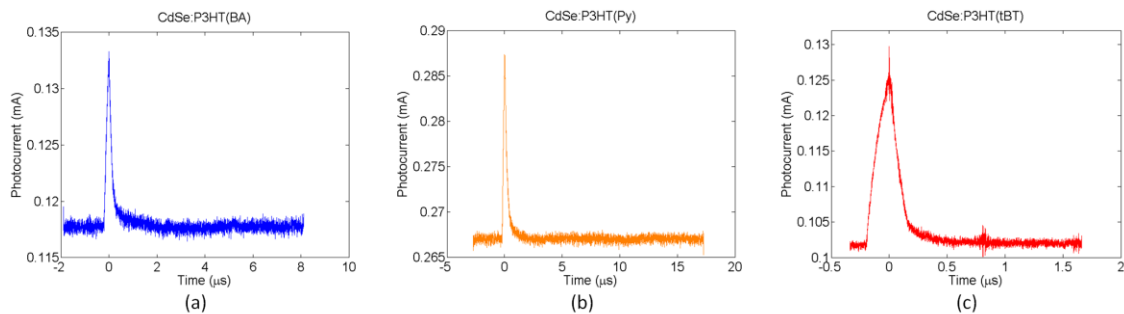


Figure 22. Transient photocurrent response for (a) P3HT:CdSe(BA), (b) P3HT:CdSe(Py), and (c) P3HT:CdSe(tBT).

The log-log plots are shown in Figures 23, 24, and 25 for each device. The linear fits provide 'transit time' values corresponding to the time taken for carriers to

transit from one electrode to another. The transit time was used to calculate mobility values for each device using the formula previously used for P3HT:PCBM device.

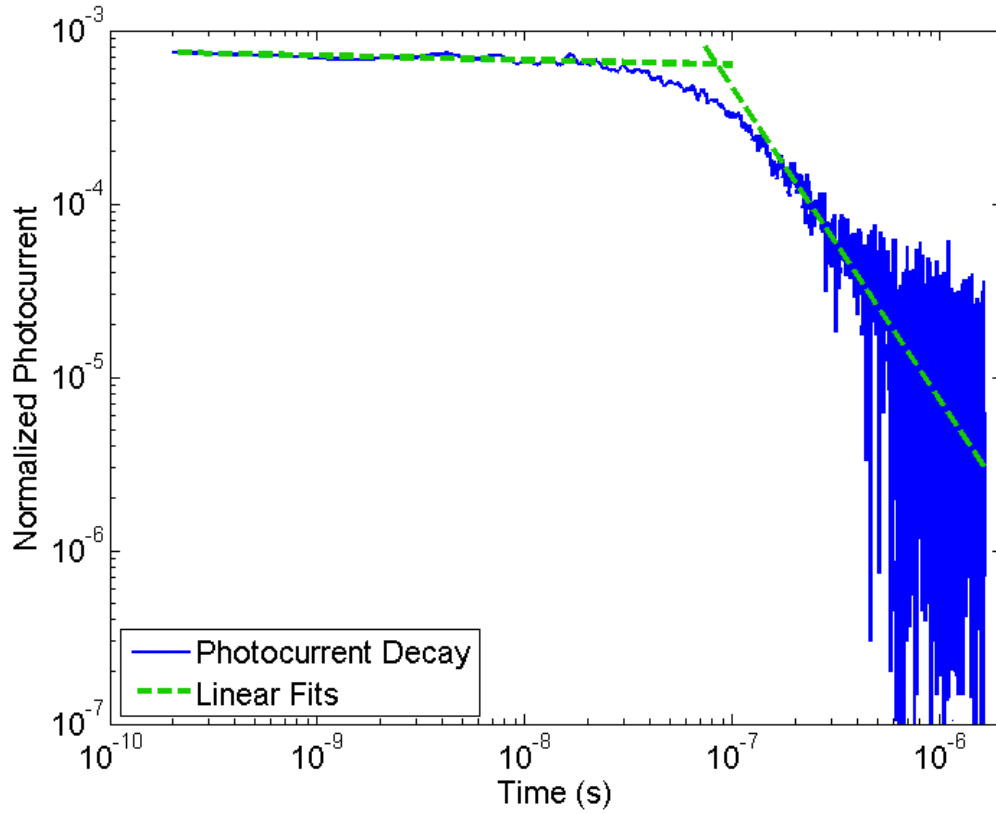


Figure 23. Double logarithmic plot for P3HT:CdSe(BA) at -3V. The intersecting linear fits give the transit time.

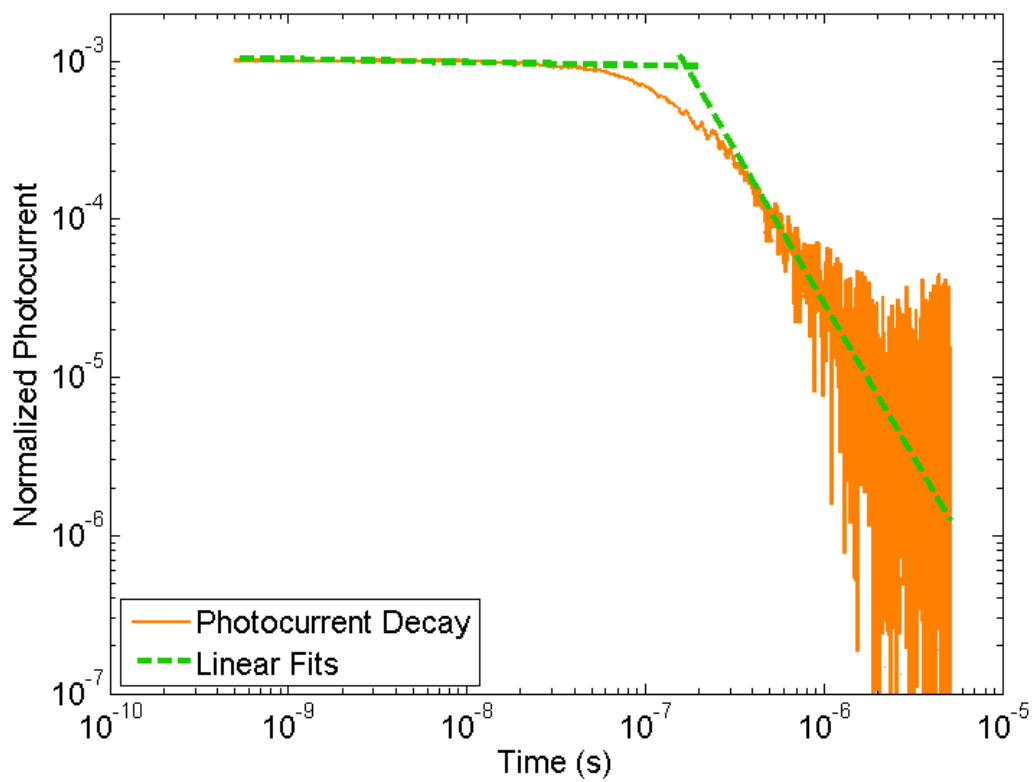


Figure 24. Double logarithmic plot for P3HT: CdSe(Py) at -3V. The intersecting linear fits give the transit time.

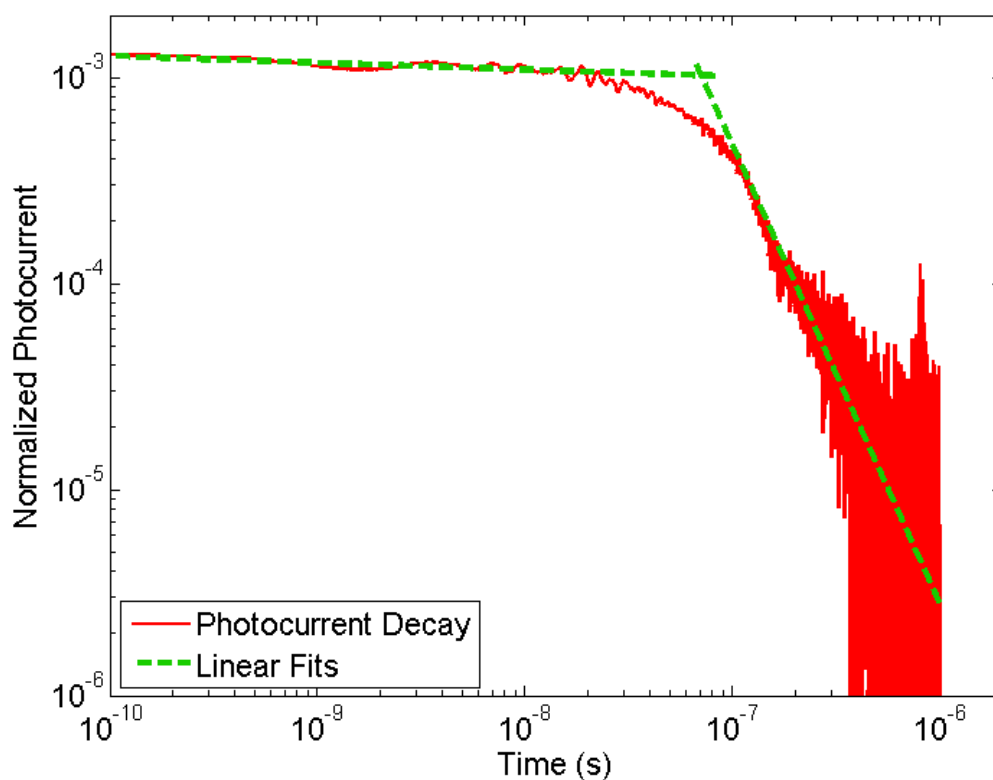


Figure 25. Double logarithmic plot for P3HT:CdSe(tBT) at -2V. The intersecting linear fits give the transit time.

The RC time constant for each transient was less than the transit times. Using the transit times obtained by the linear fits in Figures 23, 24, and 25, the carrier mobility was calculated. The mobilities are summarized below:

Ligand	PCE (%)	Mobility (cm ² /V.s)
BA	1-1.5	7×10^{-5}
NL	0.3	?
Py	2	3×10^{-5}
tBT	2-2.5	1×10^{-4}

Table 5. Charge carrier mobilities for P3HT:CdSe(BA), P3HT:CdSe(Py), and P3HT:CdSe(tBT). Mobility for P3HT:CdSe(NL) could not be determined because its thickness could not be resolved.

7. Experimental Error Calculation

In this section the error in reported value of transient photoconductivity mobility for the hole-only P3HT:PCBM device is examined.

- A. Precision error in the device transient:** There are three sets of transient photoconductivity curves for the hole-only device, and their log-log decay characteristics and results shown below:

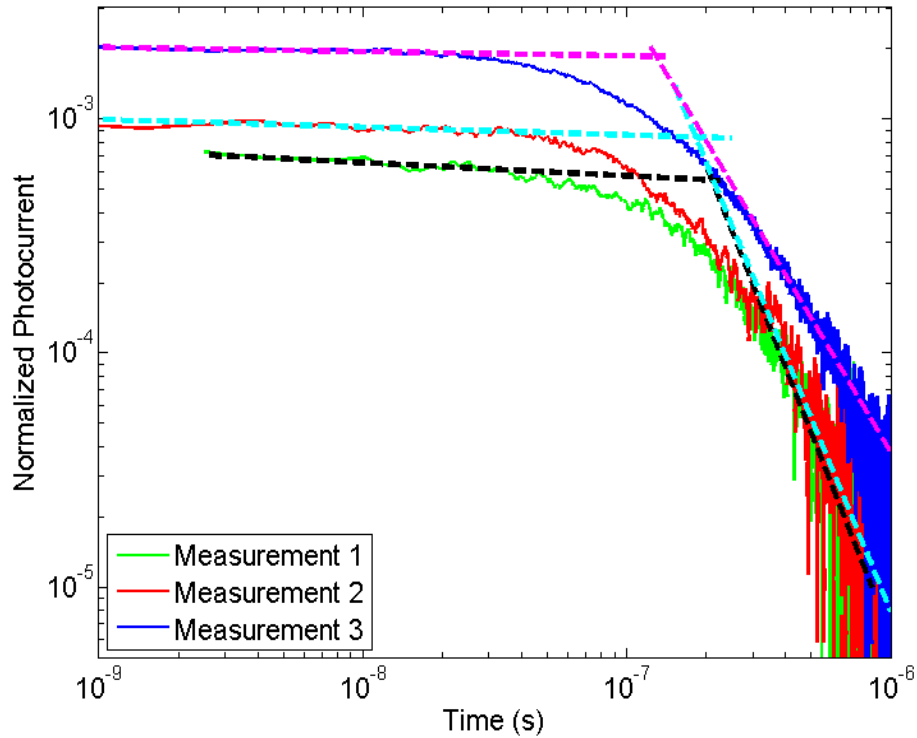


Figure 26. Double logarithmic plots for three measurements of the hole-only P3HT:PCBM device.

Measurement	μ (cm ² /V*s)
1	1x10 ⁻⁴
2	1x10 ⁻⁴
3	2x10 ⁻⁴

Table 6. Calculated values of mobility from transients shown in Figure 26.

This produces a mobility value of $1 \times 10^{-4} \pm 5 \times 10^{-5}$ cm²/V*s.

B. Precision error in capacitance and thickness measurements:

Since mobility via transient photoconductivity depends on device thickness and the built-in potential as per the formula:

$$\mu = \frac{d^2}{[2 \cdot (V_{.a} + V_{.bi}) \cdot t_{.tr}]}$$

it is important to examine the measurement errors in these variables and assess accuracy of the mobility calculations.

Error in device thickness: The active layer thickness was measured using a profilometer. The average value was recorded as 107 nm, with an error of ± 5 nm. This induces an error of $\pm 1 \times 10^{-5} \text{ cm}^2/\text{V}^*s$ in the mobility.

Error in built-in potential: The built-in potential was derived by looking at the peak capacitance value in the C-V curve as described by Mott-Schottky behavior. The increment in the voltage steps was chosen to be 0.1V, generating an error of $\pm 0.1V$. This produces a mobility error of $\pm 5 \times 10^{-6} \text{ cm}^2/\text{V}^*s$.

Clearly, the precision error in experimental reproducibility supersedes other measurement errors, producing a total error of $5 \times 10^{-5} \text{ cm}^2/\text{V}^*s$, showing that transient photoconductivity for thin films is an accurate technique.

8. Conclusion

A transient photoconductivity technique was examined for thin film organic solar cells. It was shown that the technique provides accurate and precise mobility values. A hole-only device was used for reference and its mobility was found to be $1 \times 10^{-4} \text{ cm}^2/\text{V}^*s$. The value was cross-examined using the SCLC method, which gave a mobility of $9 \times 10^{-5} \text{ cm}^2/\text{V}^*s$. After confirming the validity of the transient photocurrent method, four hybrid P3HT:CdSe solar cells with different ligands were examined using the same technique. The mobility values were found to be consistent with those previously reported in literature.

9. Future Work

9.1 Correlation with PICTS

Photo-Induced Current Transient Spectroscopy (PICTS) is a transient photoconductivity technique that has been used to identify trap states in organic and inorganic solar cells. Previously trap state emissions have been successfully reported using this technique [29]. In the future, PICTS can be used as a complimentary technique to analyze trap states for devices whose mobility was found using a similar setup. Once the mobility is measured, information about their trap emission spectra can be useful to determine whether traps play an important role in the device mobility.

9.2 Correlation with Long-Pulse Transient Response

While most transient techniques utilize nanosecond pulse excitation to study sweep-out and recombination dynamics, studying transient response after a step-function excitation ($t_{\text{pulse}} > 100 \mu\text{s}$) reveals the decay of a device in steady state. This technique has been successfully used to study and compare charge trapping and carrier lifetimes in various organic and hybrid solar cells. Studying the long-pulse transient photocurrent response under varying bias from short circuit to open voltage conditions, and under varying light intensities can show delays in charge extraction due to recombination and charge trapping [20]. Measured along with short-pulse transient photocurrent decay to find carrier mobility, the step-function transient response can be used to compare and understand the difference between the mobilities of different devices. While this technique does not reveal the trap state emission levels, it is simpler than PICTS and is useful when a comparison between devices is desired.

References

- [1] United States Environmental Protection Agency. Climate Change, July 17, 2014, from <http://www.epa.gov/climatechange/>, “<Home | Climate Change | US EPA>.”
- [2] Solar Energy Industries Association, July 2014, from <http://www.seia.org/research-resources/solar-market-insight-report-2013-year-review%5C>, “<Research & Resources | SEIA>.”
- [3] The Open PV Project, 2013, from <https://openpv.nrel.gov/>, “<The Open PV Project>.”
- [4] Best Research-Cell Efficiencies, 2014, from http://www.nrel.gov/ncpv/images/efficiency_chart.jpg, “<efficiency_chart.jpg>.”
- [5] C. Brabec, *et al.*, *Organic Photovoltaics*. Berlin: Springer, 2003.
- [6] R. Sondergaard, *et al.*, “Roll-to-roll fabrication of polymer solar cells,” *Materials Today*, vol. 15, Issue 1-2, pp. 36-49, 2012.
- [7] M.S. Ryu, *et al.*, “Effects of thermal annealing of polymer:fullerene photovoltaic solar cells for high efficiency,” *Current Applied Physics*, vol. 10, Issue 2, pp. s206-s209, 2010.
- [8] D. Chi, *et al.*, “High efficiency P3HT:PCBM solar cells with and inserted PCBM layer,” *J. Mater. Chem. C*, vol. 2, Issue 22, pp. 4383-4387, 2014.
- [9] PVCDROM, 2014, from <http://www.pveducation.org/pvcdrom>, “<Welcome to PVCDROM | PVEducation>.”
- [10] D. Chen, *et al.*, “P3HT/PCBM Bulk Heterojunction Organic Photovoltaics: Correlating Efficiency and Morphology,” *Nano Letters*, vol. 11, pp. 561-567, 2011.
- [11] G. Yu, *et al.*, “Polymer Photovoltaic Cells: Enhanced Efficiencies via a Network of Internal Donor-Acceptor Heterojunctions,” *Science*, vol. 270, pp. 1789-1791, 1995.
- [12] L. Koster, *et al.*, “Device model for the operation of polymer/fullerene bulk heterojunction solar cells,” *Physical Review B*, vol. 72, p. 085205, 2005.
- [13] S.M. Sze and K.K. Ng, *Physics of semiconductor devices*. New York: Wiley, 2005.
- [14] Ioffe Physio-Technical Institute. 2001, from <http://www.ioffe.ru/SVA/NSM/>, “<New Semiconductor Materials. Characteristics and Properties>.”
- [15] V. Coropceanu, *et al.*, “Charge Transport in Organic Semiconductors,” *Chemical Reviews*, vol. 107, Issue 4, pp. 926-952, 2007.
- [16] The A to Z of Materials. 2012, from <http://www.azom.com/article.aspx?ArticleID=5992>, “<Improved Measurement Consistency of Low Mobility Materials Using the AC Hall Effect Method>.”
- [17] J. Lindemuth and S. Mizuta, “Hall measurements on low-mobility materials and high resistivity materials,” *Proc. SPIE*, vol. 8110, Thin Film Solar Technology III, 8110I, 2011.
- [18] A. Pivrikas, *et al.*, “A Review of Charge Transport and Recombination in Polymer/Fullerene Organic Solar Cells,” *Prog. Photovolt: Res. Appl.*, vol. 15, pp. 677-696, 2007.
- [19] A. Kokil, *et al.*, “Techniques for characterization of charge carrier mobility in organic semiconductors,” *J. Polym. Sci. B Polym. Phys.*, vol. 50, pp. 1130-1144, 2012.

- [20] Z. Li, *et al.*, "Comparison of the Operation of Polymer/Fullerene, Polymer/Polymer, and Polymer/Nanocrystal Solar Cells: A Transient Photocurrent and Photovoltage Study," *Adv. Funct. Mater.*, vol. 21, pp. 1419-1431, 2011.
- [21] S. Cowan, *et al.*, "Transient photoconductivity in polymer bulk heterojunction solar cells: Competition between sweep-out and recombination," *Physical Review B*, vol. 83, p. 035205, 2011.
- [22] D. Chirvase, *et al.*, "Electrical and optical design and characterisation of regioregular poly(3-hexylthiophene-2,5diyl)/fullerene-based heterojunction polymer solar cells," *Synthetic Materials*, vol. 138, pp. 299-304, 2003.
- [23] O. Reid, *et al.*, "Space Charge Limited Current Measurements on Conjugated Polymer Films using Conductive Atomic Force Microscopy," *Nano Lett.*, vol. 8, pp. 1602-1609, 2008.
- [24] D. Chirvase, *et al.*, "Temperature dependent characteristics of poly(3 hexylthiophene)-fullerene based heterojunction organic solar cells," *J. Appl. Phys.*, vol. 93, p. 3376, 2003.
- [25] Z. Wang, *et al.*, "Carrier mobility of organic semiconductors based on current-voltage characteristics," *J. Appl. Phys.*, vol. 107, p. 034506, 2010.
- [26] Y. Shen and M. Gupta, "Investigation of electrical characteristics of P3HT:PCBM organic solar cells," *Photovoltaic Specialists Conference (PVSC), 2012 38th IEEE*, pp. 002770-002774, 2012.
- [27] Y. Shen, *et al.*, "Bulk and contact resistance in P3HT:PCBM heterojunction solar cells," *Solar Energy Materials and Solar Cells*, vol. 95, pp. 2314-2317, 2011.
- [28] V. Mihailetschi, *et al.*, "Charge Transport and Photocurrent Generation in Poly(3-hexylthiophene):Methanofullerene Bulk-Heterojunction Solar Cells," *Adv. Funct. Mater.*, vol. 16, pp. 699-708, 2006.
- [29] X. Mathew, "Photo-induced current transient spectroscopic study of traps in CdTe," *Solar Energy Materials and Solar Cells*, vol. 76, pp. 225-242, 2003.